Drug Design, Development and Therapy

Dovepress
Taylor & Francis Group

Open Access Full Text Article

ORIGINAL RESEARCH

Cytoskeleton Rearrangement Decreases Mitochondrial Fatty Acid Oxidation in Renal Tubular Epithelial Cells Contributing to Renal Fibrogenesis

Gaoling Wang[1,2], Yue Li[1], Xing Wan[1], Yu Wang[1], Huimin Niu[1,3], Enxue Tan[1], Songlin Niu[1], Xiaojian Feng[1,4], Yanjuan Hou[1], Lihua Wang[1]

[1]Department of Nephrology, Second Hospital, Shanxi Medical University, Taiyuan, People's Republic of China; [2]Department of Hospital Infection Management Office, Shanxi Bethune Hospital, Shanxi Academy of Medical Sciences, Tongji Shanxi Hospital, Third Hospital of Shanxi Medical University, Taiyuan, People's Republic of China; [3]Department of Nephrology, Heping Hospital Affiliated to Changzhi Medical College, Changzhi, People's Republic of China; [4]Department of Nephrology, Shenzhen Yantian District Hospital, Shenzhen, People's Republic of China

Correspondence: Lihua Wang, Department of Nephrology, Second Hospital, Shanxi Medical University, No.382 Wuyi Road, Taiyuan, Shanxi Province, 030000, People's Republic of China, Email lihuawang236@126.com

Purpose: The epithelial-mesenchymal transition (EMT) plays an important role in renal fibrosis. Defective fatty acid oxidation (FAO) is the metabolic hallmark in injured tubular epithelial cells (TECs) contributing to renal fibrogenesis. Dysregulated cytoskeleton is believed to be an important element of renal injury and its function has been linked to cell metabolism, but little is known about the influence of the cytoskeleton on FAO in TECs. Herein, we aimed to investigate the protective effects and molecular mechanisms of pharmacological stabilization of the cytoskeleton against unilateral ureteric obstruction (UUO) -induced renal tubulointerstitial fibrosis.

Materials and Methods: TGF-β1-treated primary tubular epithelial cells (PTECs) and UUO mice served as renal interstitial fibrosis (RIF) models, with or without pharmacological cytoskeleton stabilization by Bis-T-23 (TargetMol, T30479; 20 mg/kg/day intraperitoneally in vivo; 5 μM in vitro). Biomarkers, HE staining, PAS staining, Masson staining, Sirius red staining, and TUNEL assay were used to assess kidney function and apoptosis. Real-time quantitative PCR (qPCR), Western blotting and immunohistochemistry (IHC) were performed to measure mRNA and protein expression levels respectively. PTECs viability was assessed by CCK-8 assay. Bulk mRNA sequencing was used for transcriptomic analysis of cellular metabolism. FITC-phalloidin fluorescence staining was used to detect the cytoskeleton. Fluorescent co-staining was used to detect the interactions between lipid droplets (LDs) and mitochondria.

Results: Pharmacological stabilization of the cytoskeleton alleviated tubulointerstitial injury, functional changes and TEC damage in UUO mouse models. Stabilization of cytoskeleton restored FAO and enhanced FAO-associated respiration impaired by UUO injury. Here, we demonstrate that cytoskeleton rearrangement is a critical regulator of mitochondrial FAO in TECs both in vitro and in vivo. We further show that this cytoskeleton-dependent regulation of FAO occurs through altered interactions between LDs and mitochondria.

Conclusion: These findings indicate that cytoskeleton stabilization is required to maintain TECs metabolism and that therapeutic manipulation of cytoskeleton remodeling could protect the kidney from fibrogenesis conditions.

Keywords: cytoskeleton, fatty acid oxidation, lipid droplets, renal tubulointerstitial fibrosis, renal tubular epithelial cells

Introduction

Chronic kidney disease (CKD) is an epidemic health issue that requires global attention.[1] Renal fibrosis is a hallmark of CKD and represents a progressive scarring process that ultimately leads to end-stage renal disease (ESRD).[2] Tubulointerstitial fibrosis, a major component of renal fibrosis, is closely associated with tubular injury, inflammatory cell infiltration, and extracellular matrix (ECM) accumulation, ultimately resulting in impaired renal function.[3] Despite

Received: 28 February 2025
Accepted: 21 August 2025
Published: 4 September 2025

advancements in understanding CKD pathogenesis, effective therapeutic options targeting renal fibrosis remain limited, necessitating the exploration of new therapeutic approaches.

One of the critical mechanisms in renal fibrosis involves cytoskeletal rearrangement and the Epithelial-Mesenchymal Transition (EMT) of renal tubular epithelial cells (TECs), both of which promote a profibrotic phenotype.[4,5] During EMT, TECs lose their epithelial characteristics, such as E-cadherin expression, and gain mesenchymal markers, including α-SMA, leading to a more fibrotic cellular environment. Inhibiting this EMT process has emerged as a potential strategy to attenuate fibrosis progression.[6] Furthermore, cytoskeletal dynamics are crucial for maintaining cellular architecture and function, suggesting that cytoskeletal stabilization may be a promising therapeutic target for fibrosis.[7]

In addition to EMT and cytoskeletal changes, metabolic reprogramming, specifically fatty acid oxidation (FAO) and oxidative phosphorylation, plays a central role in TEC health and function. TECs, known for their high energy demands, are heavily reliant on FAO-driven oxidative phosphorylation to fulfill their energy requirements.[8] Reduced FAO and impaired oxidative phosphorylation are often observed in CKD, contributing to cellular energy deficits and exacerbating fibrotic processes.[9,10] Therefore, therapeutic interventions that can restore FAO and oxidative phosphorylation have the potential to mitigate TEC injury and renal fibrosis. Emerging evidence suggests cytoskeletal dynamics regulate organelle positioning and metabolic flux—including mitochondrial function—in other cell types,[11] but this interplay remains uncharacterized in renal TECs.

Bis-T-23, a small molecule known to stabilize the cytoskeleton, has shown potential in modulating cytoskeletal integrity and metabolic pathways in previous studies.[7] However, its role in renal fibrosis and its underlying mechanisms, particularly concerning FAO and oxidative phosphorylation, have not been fully elucidated. This study aims to investigate the effects of Bis-T-23 on renal fibrosis using the unilateral ureteral obstruction (UUO) mouse model, a well-established model for studying renal injury and fibrosis. We hypothesize that Bis-T-23 can alleviate renal fibrosis by stabilizing the cytoskeleton, inhibiting EMT, and restoring metabolic function in TECs. By exploring the impact of Bis-T-23 on both structural and metabolic pathways, this study seeks to provide insights into potential therapeutic strategies for addressing renal fibrosis in CKD.

Materials and Methods

Experimental Animals

Adult male C57BL/6 mice (6–8 weeks old, n=18) were purchased from Jiangsu GemPharmatech Co. Ltd. (Jiangsu, China). They were kept in the Animal Experimental Center of Shanxi Medical University, where they were given diet and water ad libitum. After 1 week of acclimation, 18 mice were randomly divided using a blind method into three groups (n=6 mice per group): a sham group, a UUO group, and a UUO + Bis-T-23 group. As previously described, after the mice were anaesthetised by intraperitoneal injection of phenobarbital (50mg/kg body weight), the left ureter was ligated in the UUO group and UUO+Bis-T-23 group, but not in the sham group. The mice were placed on a heating pad to maintain a body temperature of 37°C. The mice in the UUO+Bis-T-23 group were given Bis-T-23 suspension (TargetMol, T30479; 20 mg/kg/day in normal saline)[7] by intraperitoneal injection for 7 consecutive days from the day before modelling, while the mice in the Sham and UUO groups were given the same dose of vehicle (0.9% saline). After 7 days of treatment, the mice were fasted for 12h and anaesthetised using pentobarbital (50mg/kg body weight) by intraperitoneal injection. The left kidney was removed and then divided evenly along the across section into two parts. One part was fixed in 4% paraformaldehyde solution for tissue sectioning, and the other part was rapidly frozen and subsequently used for Western blotting and bulk mRNA sequencing. All experimental plans have been approved by animal ethics and implemented in accordance with the regulations of the Animal Experiment Ethics Review Committee of Shanxi Medical University. The entire experimental process is strictly conducted in accordance with the <Guidelines for the Care and Use of Laboratory Animals>.

Renal Pathology and Immunohistochemistry

Renal tissues were fixed in 4% paraformaldehyde overnight at 4°C, dehydrated, embedded in paraffin, 4μm-thick tissue sections were prepared for histopathological analysis. Sections were used for Hematoxylin-Eosin staining (HE), Periodic

Acid-Schiff (PAS), sirius red staining and Masson staining. PAS staining was used to score renal tubular damage, as described previously. In brief, a pathologist randomly selected 10 nonoverlapping regions of the cortical portion of each slice, and then the degree of renal tubular injury (tubular dilatation and atrophy, intratubular cast formation, inflammatory cell infiltration and interstitial widening) in each area was scored. Lesions were scored on a 0–4 scale: 0=normal; 1=mild, involvement of <25% of the cortex; 2=moderate, involvement of <25–50% of the cortex; 3=severe, involvement of <50% −75% of the cortex; 4=involving >75% of the cortex. After sirius red and Masson staining according to standard procedures, five areas in the renal cortex were randomly selected, and then the collagen-positive areas were analysed using ImageJ software (NIH, Bethesda, MD, USA).

Immunohistochemistry of renal sections was performed using the SP kit, according to the manufacturer's instructions. Labeling was visualized with 3,3′-diaminobenzidine to produce a brown color, and the sections were counterstained with hematoxylin. All corresponding antibodies are listed in Supplementary Table 1. Two independent observers performed the staining analysis under a light microscope using a blind method. Ten unrepeated fields of view (magnification Staining 40×) were randomly selected for each section to acquire images, and the collected images were quantitatively assessed for their staining intensity using ImageJ software.

TUNEL Assay

Paraffin sections of mouse kidney tissue were assayed for apoptosis using the DeadEnd™ Fluorometric TUNEL System (Promega, G3250) according to the manufacturer's instructions. Ten different fields (×400) of kidney tissue samples from each mouse were used to count the number of cells with positive TUNEL staining and then averaged.

Determination of Serum Creatinine and Urea Nitrogen Levels

Serum from mice was collected after the experiment, and then the serum creatinine and blood urea nitrogen levels were measured using the sarcosine oxidase method and the diacetyl oxime colorimetric method, respectively, according to the manufacturer's instructions.

Mouse Primary Renal Tubular Cell Culture and Measurement of Viability

PTECs were isolated from male C57BL/6 mice (2–3 weeks old). Briefly, renal tissue was dissected, placed in ice-cold Dulbecco's PBS (DPBS) and minced into pieces. Fragments were transferred to a 15 mL tube containing 10 mL of RPMI1640 medium with 200 μL of Collagenase I (Gibco, 17018029) and digested for 30 min at 37°C in a 80rpm shaker. Thereafter, 100 μL of FBS (Thermo Fisher Scientific) was added to stop the Collagenase I reaction. Cells were further sieved through a 100 μm nylon mesh, followed by 70 μm and 40 μm nylon meshes. Cells were centrifuged for 10 min at 3000g. The pellet was resuspended in 1 mL of sterile RBC lysis buffer and incubated for 2–3 min on ice. DPBS was added, followed by centrifugation for 10 min at 300. The cells were cultured in RPMI1640 supplemented with 10% fetal bovine serum (Gibco, 16000–044), 1% penicillin and streptomycin (Gibco, 15140–122), 1% insulin transferrin selenium solutions (Pricella, PB180431) and 200ng/mL transforming growth factor (Peprotech, 315–09) at 37°C and 5% CO_2. PTECs verification was performed through cytokeratin-18 immunofluorescence staining. Images were obtained using an Olympus CKX41 inverted microscope (Tokyo, Japan).

Cell Counting Kit-8 (CCK-8) Assay

PTECs cytotoxicity assessment against Bis-T-23 was performed using a Cell Counting Kit-8 (CCK-8; Boster). Briefly, after treatment, CCK-8 solution (10 μL) was added into the culture medium (100 μL) in the required wells at 37°C for 2 h. Absorbance in the wells was analyzed at 450 nm (OD450) using a microplate reader (SpectraMax i3x, Molecular Devices, San Jose, CA, USA).

Cell Culture and Treatment

PTECs extracted using the above method were separated randomly into four groups: a normal group (N), a Bis-T-23 treatment group (Bis-T-23), a TGF-β1 group and a TGF-β1+Bis-T-23 treatment group (TGF-β1+Bis-T-23). Briefly, after the cells reached 60% confluence, the medium was replaced with normal media in the absence or presence of 10ng/mL

TGF-β1 (240-B, R&D Systems) for 24h. To determine the effects of Bis-T-23 on PTECs, we pre-incubated cells with 5μM Bis-T-23 (TargetMol, T30479, dissolved in sterile DMSO) for 1 h and subsequently exposed them to 10ng/mL TGF-β1 for 23 h.

Immunofluorescence Staining of Cells

After pretreatment, PTECs were fixed with pre-cooled methanol (−20°C, 10 min), permeabilized with 0.1% Triton X-100 (RT, 10 min), and blocked with 5% BSA (RT, 1 h). Cells were incubated with anti-E-cadherin primary antibody (1:200, 4°C overnight), washed with PBS (3×5 min), then stained with Alexa Fluor 594-conjugated secondary antibody (1:400, RT, 1.5 h in dark). Following DAPI counterstaining (5 min) and mounting with antifade medium (Boster, AR1109), samples were imaged using confocal microscopy with standardized parameters.

FITC-Phalloidin Staining

The investigation of PTECs cystoskeleton was performed by using immunfluoresence technique. After incubation, medium were removed and PTECs were washed by 1×PBS (3 times for 5 min). The PTECs were fixed with 4% paraformaldehyde for 5 min, washed in 1×PBS (3 times for 5 min) and permeabilized with 0.2% Triton X-100 for 10 min, washed in 1×PBS (3 times for 5 min). The PTECs were blocked with 3% bovine serum albumin for 1 h, and stained with FITC-phalloidin (1:200) (Solarbio, CA1620), and observed it through inverted fluorescence microscope.

LDs and Mitochondrial Fluorescence Staining

To observe the interaction between LDs and mitochondria in PTECs, fluorescence staining technique was used. After incubation, medium were removed and PTECs were washed by 1×PBS (3 times for 5 min). The pre-configured BODIPY 493/503 (2256834, Thermo) working liquid (2umol/L) and Mito-Tracker Red CMXRos working liquid (200nmol/L) (C1049B, Beyotime) was added and incubated at room temperature for 20 minutes; The PTECs were fixed with 4% paraformaldehyde for 10 min, washed in 1×PBS (3 times for 5 min) and observed it through inverted fluorescence microscope.

Protein Extraction and Western Blotting

After lysing mouse kidney tissue and PTECs using radioimmunoprecipitation assay (RIPA) buffer, which was mixed with protease and phosphatase inhibitors, the tissue protein was extracted by centrifugation at 13201×g for 20 min. The extracted protein concentration was then measured using the bicinchoninic acid (BCA) method. Equal amounts of protein were separated using sodium dodecyl sulphate polyacrylamide gel electrophoresis and transferred to polyvinylidene fluoride membranes. After blocking with 5% skimmed milk, the membranes were incubated with special primary antibodies (Supplementary Table 1) overnight at 4 °C. Next, the membranes were incubated with goat anti-rabbit or mouse IgG horseradish peroxidase conjugate (HRP; 1:2000 dilution, buffer 5% skimmed milk) for 2 h at 37 °C. The membrane was then scanned using Bio-Rad's ChemiDoc MP Imaging System (Bio-Rad, Hercules, CA, USA), and finally, the immunoreactive protein bands were analyzed using ImageJ software.

Quantitative RT-PCR

Total RNA and cDNA were obtained from frozen renal cortex tissues using TRIzol (Invitrogen) and RT-qPCR kits (Thermo Fisher Scientific), according to the manufacturer's instructions. Quantitative RT-PCR was performed using SYBR Premix Ex Taq (Takara Bio Inc.) on an Agilent Mx3000P qPCR System (Agilent, Palo Alto, CA, USA). Normalization was performed using 18S rRNA. Primer sequences used for mRNA quantification are listed in Supplemental Table 2.

Statistics

All data were expressed as mean ± standard deviation (mean ± SD). Statistical analysis was performed using the statistical package SPSS for Windows, version 26.0 (IBM Corp, Armonk, NY, USA). One-way analysis of variance

(ANOVA) was used for comparisons between multiple groups, and the least significant difference (LSD) method was used for pairwise comparisons between groups. $P<0.05$ was considered to indicate a statistically significant difference.

Results

Pharmacological Stabilization of Cytoskeleton Alleviated Tubulointerstitial Injury in UUO Mouse Models

As shown in Figure 1A, HE and PAS staining of kidney sections showed that the tubular and glomerular structures of the sham group were intact, while the UUO group had severe structural disorders, including tubular dilatation, atrophy, intratubular cast formation, inflammatory cell infiltration and interstitial widening. After Bis-T-23 intervention, histopathological damage was alleviated (Figure 1A and B). Masson's trichrome and Sirius Red showed that there was significant collagen deposition in the tubulointerstitium in the UUO group, while the renal collagen deposition in the Bis-T-23 treatment group was significantly reduced (Figure 1A and C). The EMT markers showed characteristic changes: α-SMA expression was significantly increased (IHC: Figure 1A and F; WB: Figure 1H and I; PCR: Figure 1G), while E-cadherin expression was decreased as detected by all methods in the UUO group, suggesting EMT activation. Bis-T-23 reversed these changes at both protein (Figure 1H and I) and transcriptional levels (Figure 1G). Consistently, ECM markers (collagen I and fibronectin) were upregulated in UUO kidneys at protein (IHC: Figure 1A and F; WB: Figure 1H and I) and mRNA levels (Figure 1G), with Bis-T-23 showing inhibitory effects. Furthermore, Bis-T-23 partially alleviated the abnormal serum levels of creatinine and urea nitrogen (Figure 1D and E). Taken together, these data demonstrated that Bis-T-23 has a certain protective effect against renal fibrosis.

Pharmacological Stabilization of Cytoskeleton Suppresses Renal Apoptosis in UUO

Renal cell apoptosis plays a crucial role in the formation of renal fibrosis,[12] so we first measured renal apoptotic using TUNEL technology. As previously predicted, renal cell apoptosis was rarely detected under normal physiological conditions, while the number of renal cells apoptosis increased significantly in the UUO group and Bis-T-23 treatment significantly attenuated UUO-induced renal cell apoptosis (Figure 2A and B). To determine the phenotype we observed, we then measured the expression of the apoptosis hallmark proteins: Western blotting was used to determine the expression levels of apoptosis-associated proteins. Relative to the sham group, the Bax/Bcl-2 ratio and cleaved caspase-3/caspase-3 expression showed a considerable increase in the UUO group; these values were significantly lower in the Bis-T-23+UUO group (Figure 2C and D). Furthermore, immunohistochemical staining showed that the expression of Bax protein in the UUO group was significantly enhanced compared with the sham group. Compared with the UUO group, the expression of Bax in Bis-T-23 group was significantly reduced. The expression of Bcl-2 protein in the UUO group was significantly reduced. Compared with the UUO group, the expression of Bcl-2 in Bis-T-23 group was significantly enhanced (Figure 2E). These results confirmed that Bis-T-23 treatment protected against UUO-induced renal apoptosis, especially in TECs.

Pharmacological Stabilization of the Cytoskeleton Improves Transcriptomic Analysis of Cellular Metabolism and Restores FAO and Oxidative Phosphorylation Impaired by UUO Injury

In this study, bulk mRNA sequencing was used to compare gene expression between the UUO group and the UUO+Bis-T-23 group. With a significance threshold set at $P < 0.05$ and $|\log2FC|\geq1$, a total of 1381 differentially expressed genes were identified (683 upregulated and 698 downregulated) (Figure 3A). GO and KEGG pathway enrichment analyses revealed that the upregulated differentially expressed genes were significantly enriched in the fatty acid metabolism pathway (Figure 3B and C), suggesting that Bis-T-23 may inhibit renal fibrosis by transcriptionally regulating fatty acid metabolism, thereby attenuating the progression of CKD. Building on this, we further investigated the effects of Bis-T-23 on tubular energy metabolism. Given that renal tubular epithelial cells primarily rely on fatty acid oxidation (FAO)-driven oxidative phosphorylation for energy production, we hypothesized that Bis-T-23 alleviates fibrosis by rescuing FAO impairment in UUO-induced injury. As expected, Western blot results showed that Bis-T-23 treatment reversed the

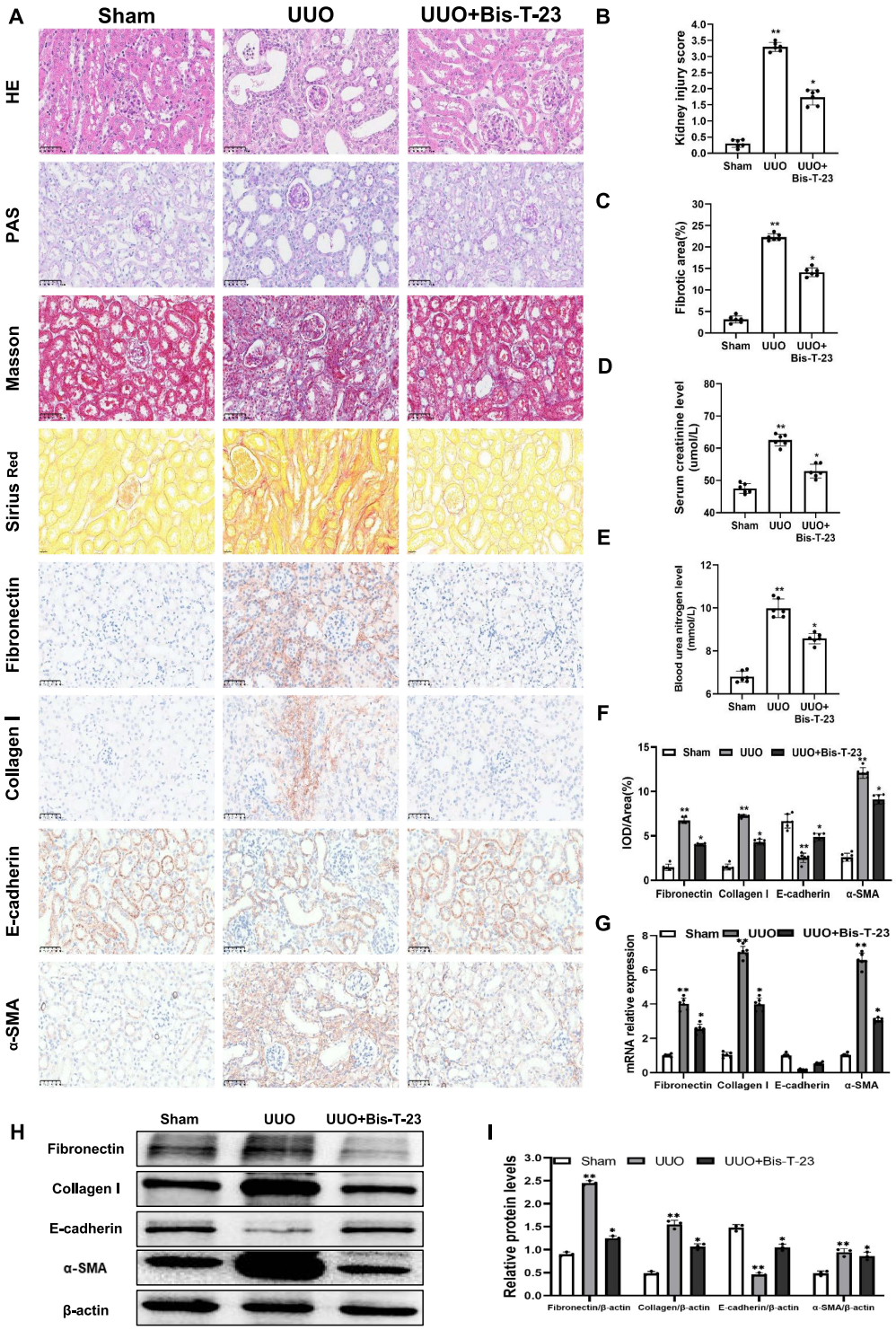

Figure 1 Cytoskeleton stabilization alleviates renal tubulointerstitial injury and fibrosis in UUO mouse models. (**A**) Representative images of kidney sections stained with Hematoxylin-Eosin (HE), Periodic Acid-Schiff (PAS), Masson's trichrome, and Sirius Red to evaluate histological damage and fibrosis. Immunohistochemical staining for fibronectin, collagen I, E-cadherin, and α-SMA was performed to assess extracellular matrix deposition, epithelial integrity, and myofibroblast activation. (The scale bar for Sirius Red is 20 μm, while it is 50 μm for HE, PAS, Masson's trichrome, and immunohistochemical staining). (**B**) Quantification of kidney injury score based on HE staining. (**C**) Quantification of fibrotic area (%) from Sirius Red staining. (**D**) Serum creatinine levels (μmol/L) in different groups. (**E**) Blood urea nitrogen levels (mmol/L) in different groups. (**F**) Immunohistochemical quantification of fibronectin, collagen I, E-cadherin, and α-SMA positive staining areas (IOD%) in different groups. (**G**) The mRNA levels of fibronectin, collagen I, E-cadherin, and α-SMA were analyzed by RT-qPCR. (**H**) Western blot analysis of fibrosis-related proteins (fibronectin, collagen (**I**) and EMT markers (E-cadherin, α-SMA) in kidney tissues from different groups, normalized to β-actin. (**I**) Quantitative analysis of fibronectin, collagen I, E-cadherin, and α-SMA protein expression ratios. Data are presented as mean±SD. **P < 0.01 vs sham group; *P < 0.05 vs UUO group.

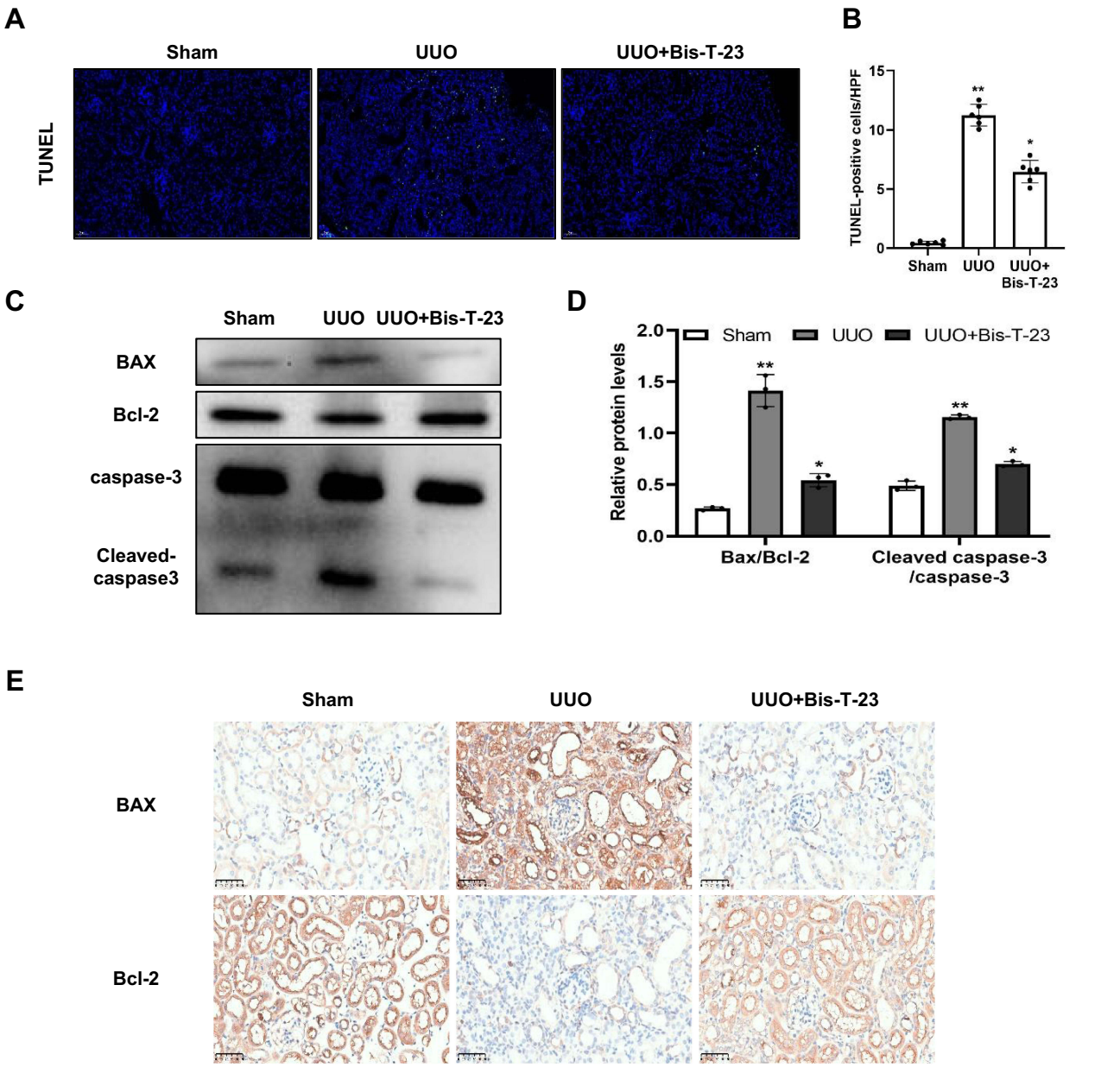

Figure 2 Cytoskeleton stabilization reduces tubular cell apoptosis in UUO mouse models. (**A**) Representative TUNEL staining images of kidney sections from sham, UUO, and UUO + Bis-T-23 groups, highlighting apoptotic cells. Scale bars, 50 μm. (**B**) Quantification of TUNEL-positive cells per high-power field (HPF). (**C**) Western blot analysis of apoptosis-related proteins BAX, Bcl-2, caspase-3, and cleaved caspase-3 in kidney tissues from different groups. (**D**) Quantitative analysis of BAX/Bcl-2 and cleaved caspase-3/caspase-3 protein expression ratios. (**E**) Immunohistochemical staining of BAX and Bcl-2 in kidney tissues, showing changes in pro-apoptotic and anti-apoptotic protein expression. Scale bars, 50 μm. Data are presented as mean±SD. **P < 0.01 vs sham group; *P < 0.05 vs UUO group.

UUO-induced downregulation of PPARα, CPT1A, and ACOX1 expression (Figure 3D and E). Immunohistochemical staining confirmed the localization of PPARα and ACOX1 in renal tubular epithelial cells (Figure 3G). Additionally, Bis-T-23 upregulated the protein levels of mitochondrial electron transport chain complexes I, III, and IV (Figure 3D and F). These results demonstrate that Bis-T-23 ameliorates UUO-induced renal injury by promoting fatty acid oxidation and oxidative phosphorylation.

https://doi.org/10.2147/DDDT.S520262

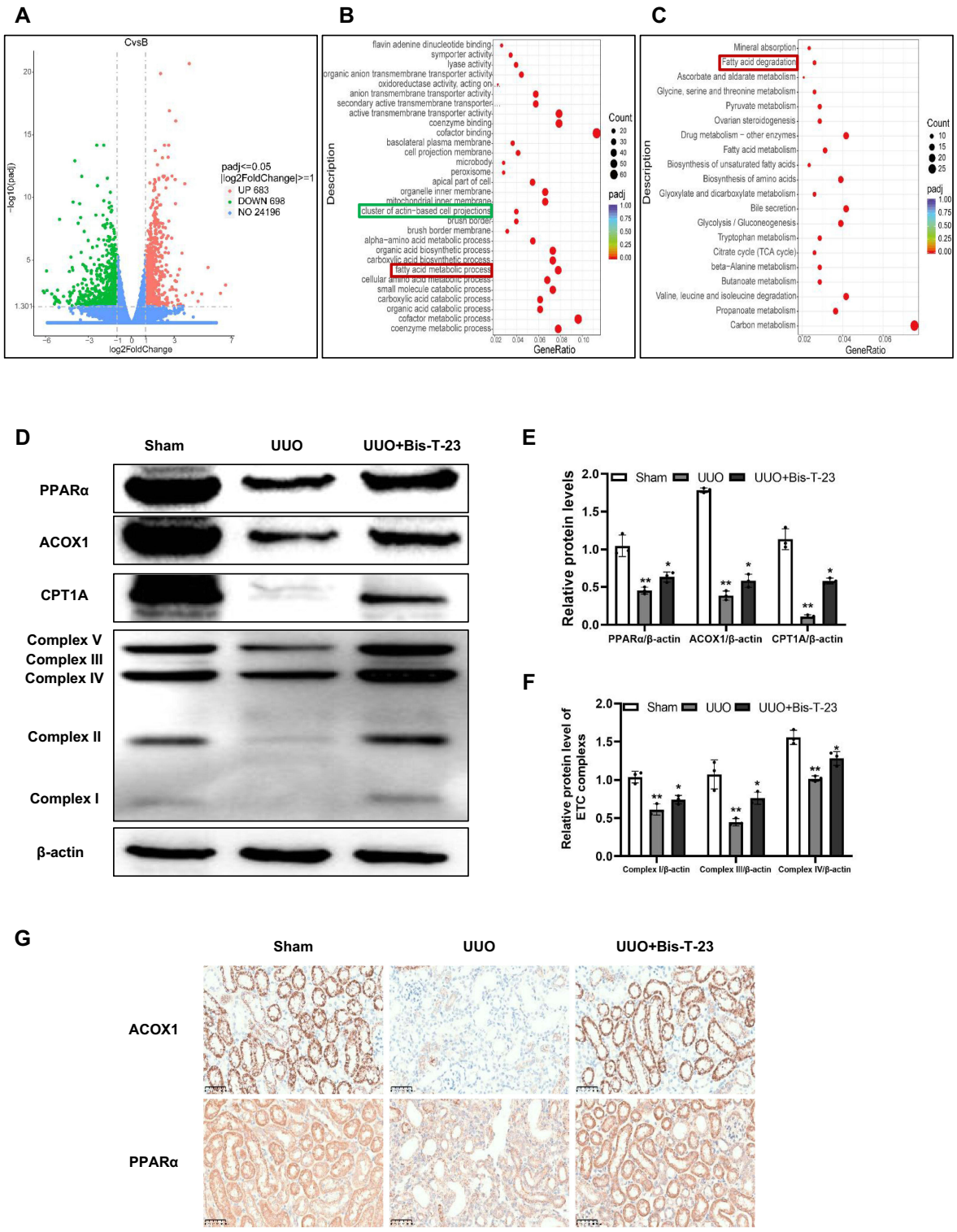

Figure 3 Cytoskeleton stabilization improves transcriptomic analysis of cellular metabolism and restores fatty acid oxidation and mitochondrial function in UUO mouse models. (**A**) According to the set statistical significance thresholds of P < 0.05 and |log2FC|≥1, 1381 differential genes were screened, of which 683 genes were significantly up-regulated and 698 genes were significantly down-regulated. (**B**) GO pathway enrichment analysis of differentially expressed genes with FAO-related pathways highlighted in red. Green borders denote cytoskeleton-related pathways demonstrating significant enrichment. (**C**) KEGG pathway enrichment analysis of differentially expressed genes with FAO-related pathways highlighted in red. (**D**) Western blot analysis of key fatty acid oxidation (FAO) enzymes and mitochondrial electron transport chain (ETC) complex proteins, including PPARα, ACOX1, CPT1A, and mitochondrial complexes I–V in kidney tissues from different groups, normalized to β-actin. (**E**) Quantitative analysis of PPARα, ACOX1, and CPT1A protein expression ratios. (**F**) Quantitative analysis of mitochondrial ETC complex protein expression ratios (complexes I, III, IV). (**G**) Representative immunohistochemical staining of PPARα and ACOX1 in kidney tissues from the different groups. Scale bars, 50 μm. Data are presented as mean±SD. **P < 0.01 vs sham group; *P < 0.05 vs UUO group.

Pharmacological Stabilization of the Cytoskeleton Protects Tubular Epithelial Cells From TGF-β1-Induced EMT, Apoptosis, FAO and Oxidative Phosphorylation

To investigate the renoprotective effects of Bis-T-23 on renal tubular epithelial cells (TECs), we established an in vitro TGF-β1-injured PTECs model. Primary tubular epithelial cells (PTECs) were authenticated by homogeneous cytokeratin-18 staining (Figure 4A), confirming isolation purity without fibroblast contamination and ensuring pathophysiological relevance. Cytotoxicity assessment via CCK-8 assay confirmed Bis-T-23 (≤10 μM) exhibited no significant cytotoxicity and demonstrated good biocompatibility (Figure 4B), and within this safe window, 5 μM Bis-T-23 pretreatment significantly reversed TGF-β1-induced cell viability damage (Figure 4C). Upon 24-hour TGF-β1 exposure, PTECs developed characteristic epithelial-mesenchymal transition (EMT): morphological shift from cobblestone-like to spindle-shaped cells, E-cadherin immunofluorescence revealing disrupted intercellular continuity, accompanied by EMT marker dysregulation (E-cadherin downregulation, α-SMA upregulation) and increased extracellular matrix deposition (elevated fibronectin/collagen; Figure 4D–F), all of which were significantly reversed by Bis-T-23 pretreatment. Western blot analysis further demonstrated elevated apoptosis markers in TGF-β1 group (increased Bax/Bcl-2 ratio and cleaved caspase-3/caspase-3; Figure 4G) and downregulated fatty acid oxidation (PPARα, CPT1A, ACOX1) and oxidative phosphorylation regulators (complexes I/III/IV; Figure 4H)—with Bis-T-23 treatment effectively normalizing these aberrant expressions, thereby rescuing apoptotic imbalance and restoring metabolic homeostasis.

Pharmacological Stabilization of the Cytoskeleton Protects Tubular Epithelial Cells From TGF-β1-Induced Cytoskeletal Disorganization and LDs-Mitochondria Interaction Disruption

To investigate whether cytoskeletal remodeling underlies impaired FAO in TECs by disrupting lipid droplet (LDs)-mitochondria interactions, we treated PTECs with TGF-β1. Consistent with our hypothesis, TGF-β1 induced cytoskeletal reorganization from radial to fascicular arrangements (Figure 5A), indicative of profibrotic phenotypic remodeling. Critically, Bis-T-23 abolished this rearrangement, confirming its anti-fibrotic function. Further mechanistic analysis revealed that Bis-T-23 robustly enhanced physical LDs-mitochondria contacts in TGF-β1-stimulated PTECs (Figure 5B). Quantitative co-localization analysis confirmed these observations (Figure 5C), demonstrating that cytoskeletal stabilization promotes LD-mitochondria interactions to support fatty acid transfer for β-oxidation.

Discussion

The cytoskeleton plays an important role in various forms of kidney diseases. Despite the many advances in understanding how cell metabolism is coupled to the actin cytoskeleton, the specific mechanism is still unknown.[11] Building upon this knowledge gap, our study systematically investigated the mechanism by which Bis-T-23 ameliorates renal fibrosis and metabolic dysfunction through cytoskeletal stabilization. Our findings demonstrate that Bis-T-23 effectively maintains structural integrity of TECs, restores FAO capacity, and inhibits apoptosis, thereby exerting anti-fibrotic effects. These findings highlight the therapeutic potential of Bis-T-23 for CKD through its multi-target mechanisms.

Studies indicate that cytoskeletal rearrangement plays a crucial role in fibrotic diseases across various organs.[13] In pulmonary fibrosis, actin cytoskeletal reorganization mediated by the ROS/RhoA-ROCK pathway induces myofibroblast transformation and collagen synthesis, influencing disease progressionlin.[14] Similarly, in liver fibrosis, myofibroblast cytoskeletal reprogramming through integrin-dependent mechanisms contributes to fibrotic development,[15] while in cardiac and hepatic fibrosis, the actin-binding protein Drebrin promotes myofibroblast fibrosis.[16] These mechanisms align with findings in renal fibrosis, where cytoskeletal stabilization has been shown to improve renal health in multiple CKD models.[7] In our UUO-induced renal fibrosis experiments, treatment with Bis-T-23 alleviated tubulointerstitial damage, reducing tubular dilation, cast formation, and inflammatory infiltration. Masson and Sirius Red staining revealed decreased collagen deposition, along with restored balance between epithelial (E-cadherin) and mesenchymal (α-SMA) markers, while renal function tests showed improved serum creatinine and urea nitrogen levels. These results are consistent with prior studies demonstrating that cytoskeletal stabilization mitigates renal fibrosis and functional impairment. Notably, Bis-T-23 simultaneously attenuates podocyte and tubular injury in the genetic murine model of Alport

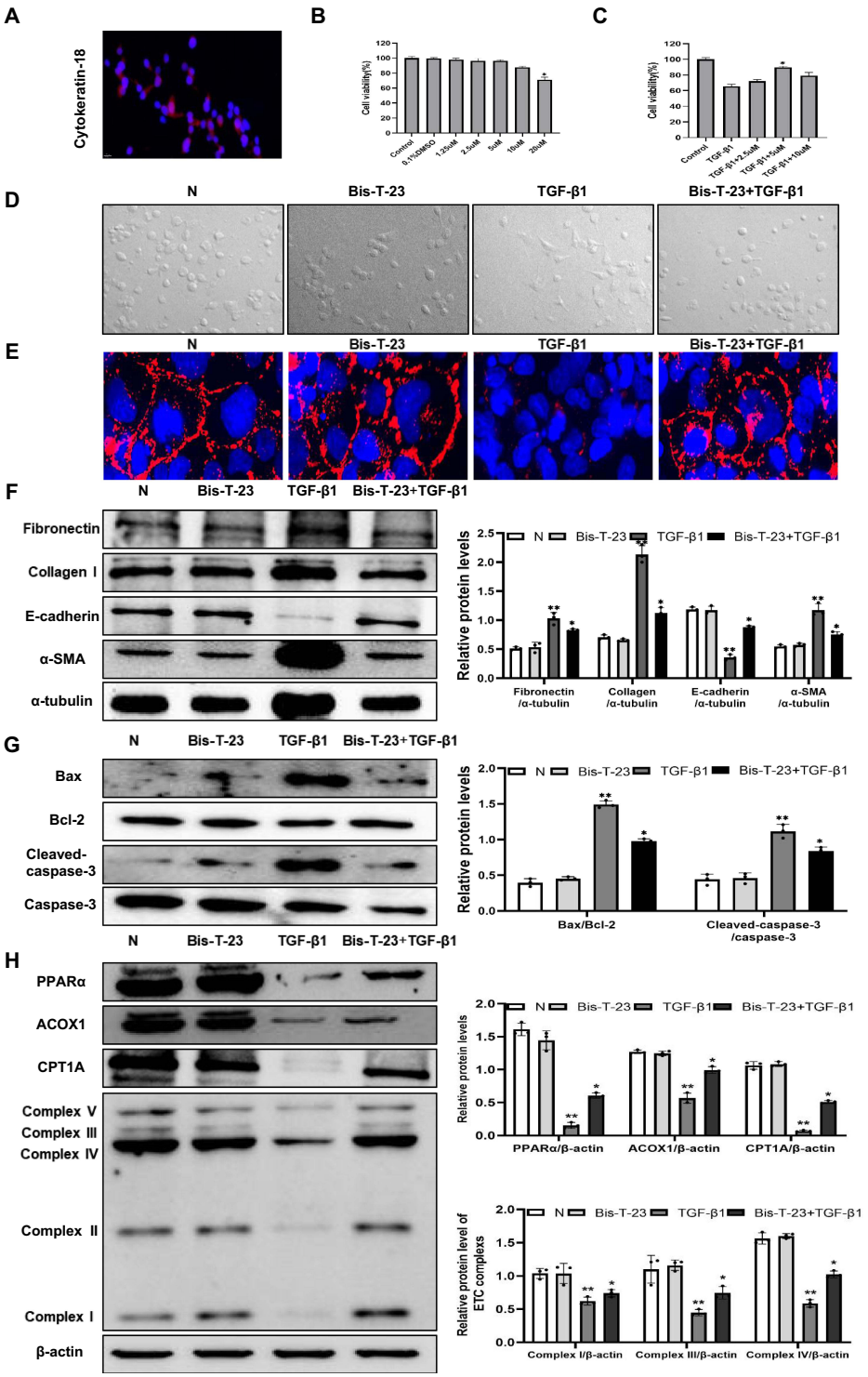

Figure 4 Cytoskeleton stabilization protects tubular epithelial cells from TGF-β1-induced EMT, apoptosis and metabolic dysfunction. (**A**) Immunofluorescence staining of cytokeratin-18 (red) confirming the epithelial origin and purity of primary tubular epithelial cells (PTECs) used for in vitro experiments, validating successful isolation of renal tubular epithelial cells. Nuclei were stained with DAPI (blue). Scale bar, 20 μm. (**B**) Cell viability of primary renal tubular epithelial cells treated with different concentrations of Bis-T-23. (**C**) Cell viability of primary renal tubular epithelial cells pre-treated with different concentrations of Bis-T-23, followed by TGF-β1 induction. (**D**) Morphological changes in tubular epithelial cells treated with normal media (N), Bis-T-23, TGF-β1, or TGF-β1+Bis-T-23. (**E**) Immunofluorescence staining of E-cadherin (red) and nuclei (DAPI, blue) to evaluate EMT induction. Scale bar, 20 μm. (**F**) Western blot analysis of fibrosis-related proteins (fibronectin, collagen I) and EMT markers (E-cadherin, α-SMA) in different treatment groups, with quantitative protein levels normalized to α-tubulin. (**G**) Western blot analysis of apoptosis-related proteins BAX, Bcl-2, caspase-3, and cleaved caspase-3 in different treatment groups. Quantitative analysis of BAX/Bcl-2 and cleaved caspase-3/caspase-3 protein expression ratios. (**H**) Western blot analysis of key fatty acid oxidation (FAO) enzymes and mitochondrial electron transport chain (ETC) complex proteins, including PPARα, ACOX1, CPT1A, and mitochondrial complexes I–V in different treatment groups, with quantitative protein levels normalized to β-actin. Data are presented as mean±SD.**P < 0.01 vs N group; *P < 0.05 vs TGF-β1 group.

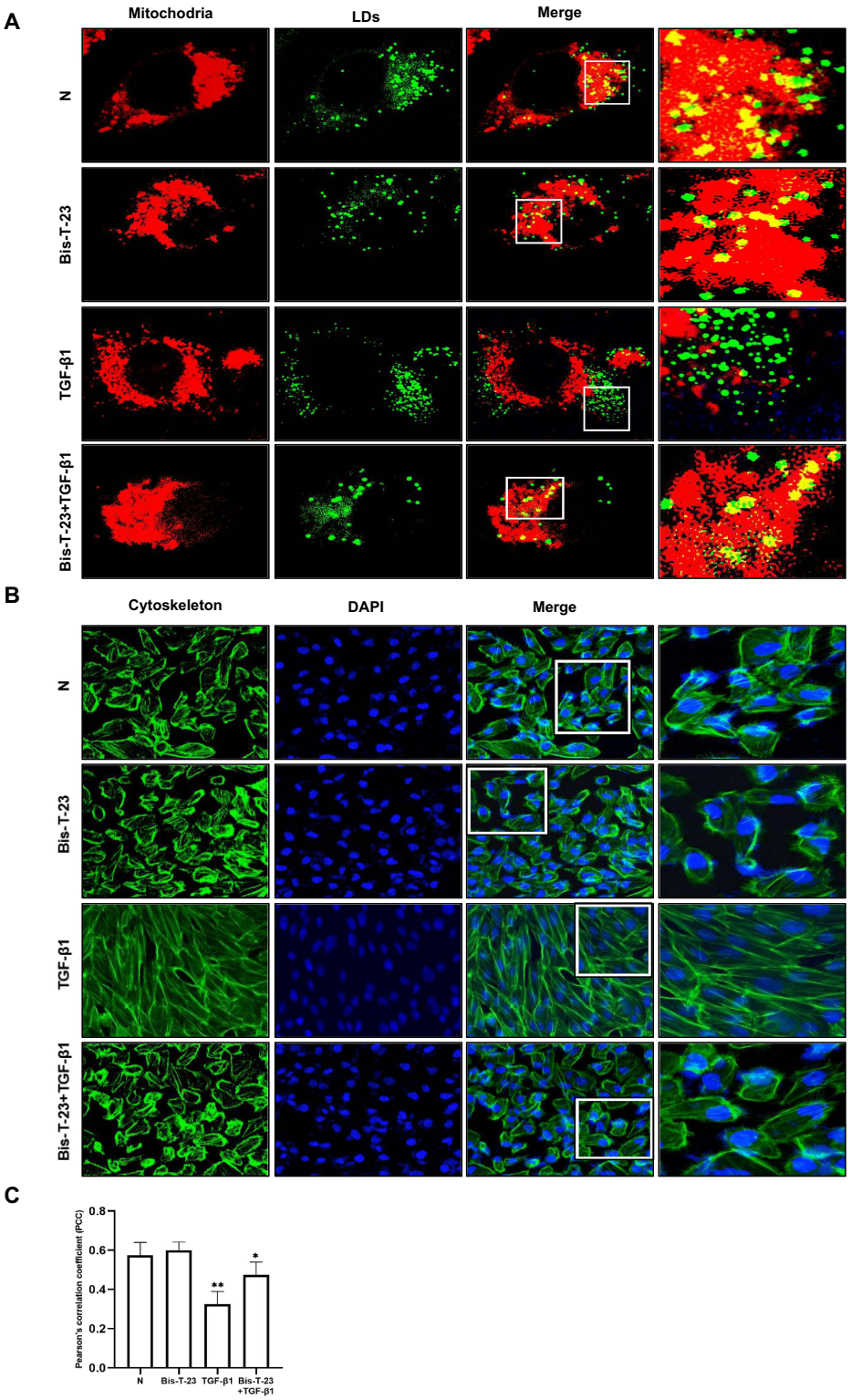

Figure 5 Cytoskeletal Stabilization Protects Tubular Epithelial Cells from TGF-β1-Induced Cytoskeletal Disorganization and LD-Mitochondria Interaction Disruption. (**A**) Representative confocal microscopy images showing mitochondria (red) and lipid droplets (LDs, green) in tubular epithelial cells treated in different treatment groups. Merged images show colocalization of mitochondria and LDs, indicating functional interaction. The inset zooms highlight the degree of LD-mitochondria interaction in each group. Scale bar, 5 μm. (**B**) Immunofluorescence staining of F-actin (green) and nuclei (DAPI, blue) to evaluate EMT induction. Nuclei were stained with DAPI (blue). The inset zooms highlight cytoskeletal architecture. Scale bar, 20 μm. (**C**) Quantitative analysis of LD-mitochondria colocalization using Pearson's correlation coefficient (PCC). Data are presented as mean±SD.**P < 0.01 vs N group; *P < 0.05 vs TGF-β1 group.

https://doi.org/10.2147/DDDT.S520262

syndrome. Bis-T-23 also preserves cell integrity via stabilization of the actomyosin cortex at the apical membrane counteracts cisplatin or iohexol-induced nephrotoxicity.[7] Our transcriptomic data demonstrate that Bis-T-23 significantly upregulates actin cytoskeleton reorganization pathways, which aligns with the cytoskeletal restructuring phenotype observed via FITC-phalloidin staining. Collectively, our findings suggest that Bis-T-23 exerts protective effects against renal fibrosis by maintaining cytoskeletal stability, thereby preventing pathological kidney remodeling, further supporting the therapeutic potential of cytoskeletal stabilization in fibrotic diseases.

The stability of the cytoskeleton plays a critical role in regulating apoptosis in renal tubular epithelial cells. Studies have shown that disruption of actin filament integrity with cytochalasin D or jasplakinolide induces apoptosis in airway epithelial cells and suggest that actin may be an early regulator of apoptosis.[17] Based on this finding, we discovered in a UUO-induced renal fibrosis model that Bis-T-23 blocks apoptosis signaling by maintaining cytoskeletal stability. Its mechanism includes downregulating the Bax/Bcl-2 ratio and cleaved-caspase3 levels, thereby reducing apoptosis-related protein expression. These findings reveal that Bis-T-23 could inhibit TEC apoptosis by stabilizing the cytoskeleton, effectively protecting renal tubular epithelial cell function and alleviating renal tissue damage.

FAO and oxidative phosphorylation are essential for the high energy demands of TECs.[18] One study of evidence from 53 patients with CKD and multiple animal models showed impaired mitochondrial fatty acid oxidation in renal TECs in advanced CKD, and impaired mitochondrial fatty acid oxidation exacerbated mesenchymal transdifferentiation, inflammatory responses, and promoted fibrosis progression in TECs. Restoration of mitochondrial fatty acid metabolism in TECs can improve interstitial lesions in CKD.[8] PPARα is highly expressed in tubular cells, regulating CPT1A expression and fatty acid oxidation. In folate-induced renal injury model, the use of PPARα agonist fenofibrate can significantly increase the expression of FAO key enzymes CPT1A and ACOX1, while reducing renal cell apoptosis, renal injury, and fibrosis.[19] Our transcriptomic analysis revealed that Bis-T-23 treatment significantly upregulated genes involved in fatty acid metabolic pathways and mitochondrial oxidative phosphorylation. This transcriptional reprogramming was functionally validated by the restoration of key FAO regulators (PPARα, CPT1A, and ACOX1) and mitochondrial electron transport chain complexes (I, III, and IV). Immunohistochemical results further confirmed the specific localization of PPARα and ACOX1 expression in TECs, demonstrating their crucial role in mediating energy metabolism. Collectively, these findings indicate that Bis-T-23 treatment effectively restored FAO and mitochondrial function, counteracting the metabolic disruption caused by UUO injury.

TGF-β is one of the important profibrotic cytokines, and its mediated abnormal activation of signaling pathways is the main pathophysiological mechanism of renal interstitial fibrosis and acute kidney injury.[20] The interactions between mitochondria and the cytoskeleton have been found to alter mitochondrial function.[21] Our in vitro experiments with TGF-β1-treated PTECs demonstrated that cytoskeletal reorganization is associated with impaired FAO and mitochondrial function. TGF-β1 induced an EMT phenotype in PTECs, characterized by reduced E-cadherin and increased α-SMA levels, accompanied by cytoskeletal rearrangement from radial to fascicular orientation. Bis-T-23 treatment inhibited these EMT-related changes, indicating that cytoskeletal stability may prevent the metabolic and structural alterations associated with fibrosis. The interaction between lipid droplets and mitochondria is the structural basis of fatty acid storage and oxidation.[22] Previous studies have shown that the interlinking of LDs with mitochondrial membrane can decompose lipids in lipid droplets into mitochondria for β-oxidation function.[23] Dysregulation of the interaction between LDs and mitochondria can lead to a variety of metabolic diseases. For example, the dysregulation of LDs-mitochondrial cross-talk function in obesity and diabetes can lead to changes in lipid metabolism and insulin resistance.[24,25] Impaired LDs-mitochondrial interaction can lead to lipid accumulation and metabolic stress in non-alcoholic fatty liver disease.[26,27] Dysregulation of LDs-mitochondrial interactions has also been associated with cardiovascular diseases and neurodegenerative diseases.[28] Under TGF-β1 stimulation, Bis-T-23 significantly enhanced LD-mitochondria interactions and promoted both FAO and oxidative phosphorylation in injured PTECs, as evidenced by increased LD-mitochondria colocalization and upregulation of key metabolic markers (PPARα, CPT1A, ACOX1, and mitochondrial complexes I, III, and IV). Importantly, our study mechanistically links actin cytoskeleton stabilization to the restoration of FAO and mitochondrial function, at least in part through promoting LD-mitochondrial interactions in injured tubular epithelial cells.

Overall, our findings demonstrate that cytoskeletal stabilization plays a pivotal role in mitigating renal fibrosis by simultaneously maintaining both the structural integrity and metabolic homeostasis of renal tubular epithelial cells. Bis-T-23 shows therapeutic potential through multiple mechanisms: stabilizing cytoskeleton, restoring fatty acid oxidation, and inhibiting apoptosis, effectively reducing tubular damage and fibrosis in UUO models. This dual targeting of cellular architecture and energy metabolism presents a novel CKD treatment approach. Further research should validate these findings in other renal injury models and elucidate cytoskeleton-mitochondria interactions to facilitate clinical development.

Data Sharing Statement

The data used in the study can be made available by the corresponding author upon reasonable request.

Author Contributions

All authors made a significant contribution to the work reported, whether that is in the conception, study design, execution, acquisition of data, analysis and interpretation, or in all these areas; took part in drafting, revising or critically reviewing the article; gave final approval of the version to be published; have agreed on the journal to which the article has been submitted; and agree to be accountable for all aspects of the work.

Funding

This work was supported by grants from the National Natural Science Foundation of China [grant number 82170746] [LHW] and "PRO Run" Fund of the Nephrology Group of CEBM [KYJ202206-0003-4][YJH].

Disclosure

All authors declare that there are no competing interests.

References

1. Lameire NH, Levin A, Kellum JA, et al. Harmonizing acute and chronic kidney disease definition and classification: report of a kidney disease: improving global outcomes (KDIGO) consensus conference. *Kidney Int*. 2021;100(3):516–526. doi:10.1016/j.kint.2021.06.028
2. Feng X, Zhang J, Yang R, et al. The novel peptide PEP-Z-2 potentially treats renal fibrosis in vivo and in vitro by regulating TGF-β/Smad/AKT/MAPK signaling. *Eur J Pharmacol*. 2024;982:176942. doi:10.1016/j.ejphar.2024.176942
3. Wu H, Z Qiu, Wang L, et al. Renal fibrosis: SIRT1 still of value. *Biomedicines*. 2024;12(9):1942. doi:10.3390/biomedicines12091942
4. Djudjaj S, Boor P. Cellular and molecular mechanisms of kidney fibrosis. *Mol Aspects Med*. 2019;65:16–36. doi:10.1016/j.mam.2018.06.002
5. H Sun, Zhao A, Li M, et al. Interaction of calcium binding protein S100A16 with myosin-9 promotes cytoskeleton reorganization in renal tubulointerstitial fibrosis. *Cell Death Dis*. 2020;11(2):146. doi:10.1038/s41419-020-2337-z
6. Meng P, C Liu, Li J, et al. CXC chemokine receptor 7 ameliorates renal fibrosis by inhibiting β-catenin signaling and epithelial-to-mesenchymal transition in tubular epithelial cells. *Ren Fail*. 2024;46(1):2300727. doi:10.1080/0886022X.2023.2300727
7. Mukherjee K, Gu C, Collins A, et al. Simultaneous stabilization of actin cytoskeleton in multiple nephron-specific cells protects the kidney from diverse injury]. *Nat Commun*. 2022;13(1):2422. doi:10.1038/s41467-022-30101-4
8. Kang HM, Ahn SH, Choi P, et al. Defective fatty acid oxidation in renal tubular epithelial cells has a key role in kidney fibrosis development. *Nat Med*. 2015;21(1):37–46. doi:10.1038/nm.3762
9. Gewin LS. Renal fibrosis: primacy of the proximal tubule. *Matrix Biol*. 2018;68-69:248–262. doi:10.1016/j.matbio.2018.02.006
10. Wilkening A, Krappe J, Mühe AM, et al. C-C chemokine receptor type 2 mediates glomerular injury and interstitial fibrosis in focal segmental glomerulosclerosis. *Nephrol Dial Transplant*. 2020;35(2):227–239. doi:10.1093/ndt/gfy380
11. Dewane G, Salvi AM, Demali KA. Fueling the cytoskeleton - links between cell metabolism and actin remodeling. *J Cell Sci*. 2021;134(3). doi:10.1242/jcs.248385
12. Zhang Y, Lv L, Zhou Z, et al. Piezo1 facilitates the initiation and progression of renal fibrosis by mediating cell apoptosis and mitochondrial dysfunction. *Ren Fail*. 2024;46(2):2415519. doi:10.1080/0886022X.2024.2415519
13. Gu C, Chang J, Shchedrina VA, et al. Regulation of dynamin oligomerization in cells: the role of dynamin-actin interactions and its GTPase activity. *Traffic*. 2014;15(8):819–838. doi:10.1111/tra.12178
14. Ni J, Dong Z, W Han, et al. The role of RhoA and cytoskeleton in myofibroblast transformation in hyperoxic lung fibrosis. *Free Radic Biol Med*. 2013;61:26–39. doi:10.1016/j.freeradbiomed.2013.03.012
15. Xi Y, Lacanna R, Ma HY, et al. A WISP1 antibody inhibits MRTF signaling to prevent the progression of established liver fibrosis. *Cell Metab*. 2022;34(9):1377–93.e8. doi:10.1016/j.cmet.2022.07.009
16. Hironaka T, Takizawa N, Yamauchi Y, et al. The well-developed actin cytoskeleton and Cthrc1 expression by actin-binding protein drebrin in myofibroblasts promote cardiac and hepatic fibrosis. *J Biol Chem*. 2023;299(3):102934. doi:10.1016/j.jbc.2023.102934
17. White SR, Williams P, R Wojcikk, et al. Initiation of apoptosis by actin cytoskeletal derangement in human airway epithelial cells. *Am J Respir Cell Mol Biol*. 2001;24(3):282–294. doi:10.1165/ajrcmb.24.3.3995

18. Li Z, Lu S, Li X. The role of metabolic reprogramming in tubular epithelial cells during the progression of acute kidney injury. *Cell Mol Life Sci*. 2021;78(15):5731–5741. doi:10.1007/s00018-021-03892-w
19. Takahashi K, Kamijo Y, Hora K, et al. Pretreatment by low-dose fibrates protects against acute free fatty acid-induced renal tubule toxicity by counteracting PPARα deterioration. *Toxicol Appl Pharmacol*. 2011;252(3):237–249. doi:10.1016/j.taap.2011.02.012
20. Meng XM, NIKOLIC-Paterson DJ, Y Lanh. TGF-β: the master regulator of fibrosis. *Nat Rev Nephrol*. 2016;12(6):325–338. doi:10.1038/nrneph.2016.48
21. B Fcasafuza, C Derossim, Bruno L. Mitochondrial cellular organization and shape fluctuations are differentially modulated by cytoskeletal networks. *Sci Rep*. 2023;13(1):4065. doi:10.1038/s41598-023-31121-w
22. Thiam AR, Dugail I. Lipid droplet-membrane contact sites - from protein binding to function. *J Cell Sci*. 2019;132(12). doi:10.1242/jcs.230169
23. Veliova M, Petcherski A, Liesa M, et al. The biology of lipid droplet-bound mitochondria. *Semin Cell Dev Biol*. 2020;108:55–64. doi:10.1016/j.semcdb.2020.04.013
24. C Lin, chen J, Hu M, et al. Sesamol promotes browning of white adipocytes to ameliorate obesity by inducing mitochondrial biogenesis and inhibition mitophagy via β3-AR/PKA signaling pathway. *Food Nutr Res*. 2021;65:10–29219.
25. Valent AM, Choi H, Kolahi KS, et al. Hyperglycemia and gestational diabetes suppress placental glycolysis and mitochondrial function and alter lipid processing. *FASEB J*. 2021;35(3):e21423. doi:10.1096/fj.202000326RR
26. Talari NK, Mattam U, Meher NK, et al. Lipid-droplet associated mitochondria promote fatty-acid oxidation through a distinct bioenergetic pattern in male Wistar rats. *Nat Commun*. 2023;14(1):766. doi:10.1038/s41467-023-36432-0
27. Afonso MB, Islam T, Magusto J, et al. RIPK3 dampens mitochondrial bioenergetics and lipid droplet dynamics in metabolic liver disease. *Hepatology*. 2023;77(4):1319–1334. doi:10.1002/hep.32756
28. Montaigne D, Butruille L, Staels B. PPAR control of metabolism and cardiovascular functions. *Nat Rev Cardiol*. 2021;18(12):809–823. doi:10.1038/s41569-021-00569-6